Journal of Inorganic Biochemistry 147 (2015) 116–125

Contents lists available at ScienceDirect

Journal of Inorganic Biochemistry

journal homepage: www.elsevier.com/locate/jinorgbio

Expanding the family of heteroleptic oxidovanadium(IV) compounds with salicylaldehyde semicarbazones and polypyridyl ligands showing anti-*Trypanosoma cruzi* activity

Gonzalo Scalese [a], Julio Benítez [a], Santiago Rostán [a], Isabel Correia [b], Lara Bradford [a], Marisol Vieites [a], Lucía Minini [c], Alicia Merlino [c], E. Laura Coitiño [c], Estefania Birriel [d], Javier Varela [d], Hugo Cerecetto [d], Mercedes González [d], João Costa Pessoa [b], Dinorah Gambino [a,*]

[a] Cátedra de Química Inorgánica, Facultad de Química, Universidad de la República, Gral. Flores 2124, 11800 Montevideo, Uruguay
[b] Centro de Química Estrutural, Instituto Superior Técnico, Universidade de Lisboa, Av Rovisco Pais, 1049-001 Lisboa, Portugal
[c] Laboratorio de Química Teórica y Computacional, Facultad de Ciencias, Universidad de la República, Iguá 4225, 11400, Uruguay
[d] Grupo de Química Medicinal, Laboratorio de Química Orgánica, Facultad de Ciencias-Facultad de Química, Universidad de la República, Iguá 4225, 11400 Montevideo, Uruguay

ARTICLE INFO

Article history:
Received 11 November 2014
Received in revised form 1 March 2015
Accepted 4 March 2015
Available online 12 March 2015

Keywords:
Oxidovanadium(IV) complexes
Salicylaldehyde semicarbazones
Trypanosoma cruzi
Tetramethylphenanthroline
DNA interaction

ABSTRACT

Searching for prospective vanadium-based drugs for the treatment of Chagas disease, a new series of heteroleptic [$V^{IV}O$(L-2H)(NN)] compounds was developed by including the lipophilic 3,4,7,8-tetramethyl-1,10-phenanthroline (tmp) NN ligand and seven tridentate salicylaldehyde semicarbazone derivatives (L1–L7). The compounds were characterized in the solid state and in solution. EPR spectroscopy suggests that the NN ligand is bidentate bound through both nitrogen donor atoms in an axial–equatorial mode. The EPR and ^{51}V-NMR spectra of aerated solutions at room temperature indicate that the compounds are stable to hydrolysis and that no significant oxidation of V^{IV} to V^{V} takes place at least in 24 h. The complexes are more active in vitro against *Trypanosoma cruzi*, the parasite responsible for Chagas disease, than the reference drug Nifurtimox and most of them are more active than previously reported [$V^{IV}O$(L-2H)(NN)] complexes of other NN co-ligands. Selectivity towards the parasite was analyzed using J-774 murine macrophages as mammalian cell model. Due to both, high activity and high selectivity, L2, L4, L5 and L7 complexes could be considered new hits for further drug development. Lipophilicity probably plays a relevant role in the bioactivity of the new compounds. The [$V^{IV}O$(L-2H)(NN)] compounds were designed aiming DNA as potential molecular target. Therefore, the novel L1–L7 tmp complexes were screened by computational modeling, comparing their DNA-binding features with those of previously reported [$V^{IV}O$(L-2H)(NN)] compounds with different NN co-ligands. Whereas all the complexes interact well with DNA, with binding modes and strength tuned in different extents by the NN and semicarbazone co-ligands, molecular docking suggests that the observed anti-*T. cruzi* activity cannot be explained upon DNA intercalation as the sole mechanism of action.

1. Introduction

Chagas disease (American trypanosomiasis) is an endemic illness that affects around 10 million people in Latin America, mainly living in poverty-stricken areas. It causes more deaths than any other parasitic disease in this region and is considered by WHO as one of the 17 neglected diseases due to lack of interest in the development of new drugs shown by the pharmaceutical industry. Moreover, Chagas disease is becoming an emerging health problem in non-endemic areas, such as United States, Australia and some European countries, because of growing population movements. The disease is produced by the protozoan parasite *Trypanosoma cruzi* (*T. cruzi*) and transmitted to the mammalian host through the bite of specific triatomine bugs. Although the occurrence of acute cases has diminished due to efforts in controlling the vector transmission undertaken by the countries involved in the WHO Southern Cone Initiative, more efficient and less toxic drugs capable of circumventing increasing drug resistance are urgently needed to treat chagasic patients.

The current chemotherapies are based on the old nitroaromatic drugs Benznidazole and Nifurtimox. However, both show several toxic effects on the patients and almost no activity in the chronic phase of the disease. Nevertheless, only very few new compounds have advanced to clinical trials, since their introduction in the clinical practice more than 40 years ago [1–5].

The development of bioactive metal compounds has demonstrated to be a promising approach in the search for new antiparasitic drugs. This strategy has led to the identification of some prospective metal-

* Corresponding author. Tel.: +598 29249739; fax: +598 29241906.
E-mail address: dgambino@fq.edu.uy (D. Gambino).

http://dx.doi.org/10.1016/j.jinorgbio.2015.03.002
0162-0134/

based drugs against highly prevalent parasitic illnesses, such as Chagas disease, malaria, leishmaniasis and amoebiasis [6–10]. The biological relevance of vanadium has led to increasing research on the potential medicinal uses of its compounds [11] and many vanadium-based prospective drugs have been proposed towards the treatment of several types of diseases. Traditionally the research on vanadium medicinal chemistry has focused on improving biodistribution and tolerability of the vanadium insulin-enhancing core or on the development of antitumor compounds [12–17]. More recently, some research groups began to dedicate efforts for the development of vanadium prospective agents against parasites that provoke some of the most prevalent parasitic illnesses [16–18].

In particular, our group has been working on the rational design of oxidovanadium(IV)-based compounds bearing activity against *T. cruzi* by including polypyridyl ligands (NN) having DNA intercalating capacity. This strategy points out at DNA as a potential parasite target and was inspired by two main facts: i) compounds able to modify nucleic acids have shown high interest for anti-tumor drug design and ii) highly proliferative cells, such as tumor cells and trypanosomatid parasites, show many metabolic similarities [19]. In particular, it is well known that many compounds that efficiently interact with DNA also exert anti-trypanosomal activity and that different homoleptic and heteroleptic oxidovanadium(IV) compounds with polypyridyl ligands have shown antitumoral properties [20–25]. Under this strategy two families of structurally related compounds with the formulae $[V^{IV}O(SO_4)(H_2O)_2(NN)]$ and $[V^{IV}O(L\text{-}2H)(NN)]$, have been synthesized, fully characterized and their biological activity evaluated on the parasite [18,26–32]. The series of twenty five heteroleptic $[V^{IV}O(L\text{-}2H)(NN)]$ compounds, where L are the tridentate salicylaldehyde semicarbazone derivatives L1–L5 (Fig. 1) and NN is either dipyrido[3,2-*a*:2′,3′-*c*]phenazine (dppz), 2,2′-bipyridine (bipy), 1,10-phenanthroline (phen), 5-amine-1,10-phenanthroline (aminophen) or 5,6-epoxy-5,6-dihydro-1,10-phenanthroline (epoxyphen), included several compounds with very interesting biological properties. Namely, most of the $V^{IV}O$-compounds were more active than Nifurtimox. Moreover, in general they were several-fold more active than the polypyridyl ligands included in their coordination spheres. The in vitro anti *T. cruzi* activity resulted mainly dependent on the nature of the NN ligand and almost independent of the chemical nature of the substituents R_1 and R_2 in the salicylaldehyde moiety (Fig. 1). Nevertheless, the brominated semicarbazone ligands tend to generate the most active compounds in each series. The phen, epoxyphen and aminophen series showed very high selectivity to the parasite in respect to mammalian cell models.

Having twenty five structurally related compounds, a QSAR study was carried out to get a design guide for further drug development. The results highlighted the relevance of the lipophilicity of the compounds and of the structure of the NN co-ligand on the anti-*T. cruzi* effect. The π-expanded systems dppz, phen and phen derivatives may intercalate between base pairs of DNA. Moreover, the highly electrophilic epoxyphen may react with protein nucleophiles and DNA through the epoxide-moiety, while the nucleophilic aminophen may react/interact with biological electrophiles through the amino moiety. The QSAR study led to a design guide for the development of new compounds, with improved biological profiles [31,32].

In respect to the mechanism of action of the compounds, their interaction with DNA was assessed through different techniques: agarose gel electrophoresis, viscosity measurements and atomic force microscopy (AFM) [18,26–32]. In addition, a metabolomic study carried out by incubating the parasite with the two most active $V^{IV}O$-compounds pointed the mitochondrion and/or related enzymatic systems as potential targets for these complexes. In addition, coordination to vanadium may improve bioavailability due to increased lipophilicity of the phenanthroline derivatives upon coordination [32].

In the current work we further expand the series of $[V^{IV}O(L\text{-}2H)(NN)]$ compounds by including the more lipophilic 3,4,7,8-tetramethyl-1,10-phenanthroline (tmp, Fig. 1) as NN ligand and by enlarging the previous group of semicarbazone ligands (L1–L5) with the inclusion of two new halogenated derivatives: 5-chlorosalicylaldehyde semicarbazone (L6) and 3,5-dibromosalicylaldehyde semicarbazone (L7). These structural modifications were designed to further evaluate the effect of lipophilicity and the presence of halogen substituents on the anti-*T. cruzi* activity.

Aiming to get a deeper insight into the probable mechanism of action across the whole family of compounds, computational modeling was carried out to compare the ability of each of the six series of complexes with different NN co-ligands to intercalate DNA. For this purpose DNA molecular docking was assessed for the seven new tmp complexes and for the head of each of the previously reported $[V^{IV}O(L\text{-}2H)(NN)]$ series (L = L1; NN = bipy, phen, dppz, aminophen or epoxyphen).

2. Materials and methods

2.1. Materials

All common laboratory chemicals were purchased from commercial sources and used without further purification. Semicarbazone ligands L1–L7 (Fig. 1) were synthesized from an equimolar mixture of the corresponding aldehyde and semicarbazide and characterized by C, H and N elemental analyses, and FTIR spectroscopy [31–36].

2.2. Syntheses of the oxidovanadium(IV) complexes, $[V^{IV}O(L\text{-}2H))(tmp)]$, *1*–*7*

The $[V^{IV}O(L\text{-}2H)(tmp)]$ complexes, where L = salicylaldehyde semicarbazone (L1), 5-bromosalicylaldehyde semicarbazone (L2), 2-hydroxy-3-methoxybenzaldehyde semicarbazone (L3), 3-ethoxysalicylaldehyde semicarbazone (L4), 5-bromo-2-hydroxy-3-methoxybenzaldehyde semicarbazone (L5), 5-chlorosalicylaldehyde

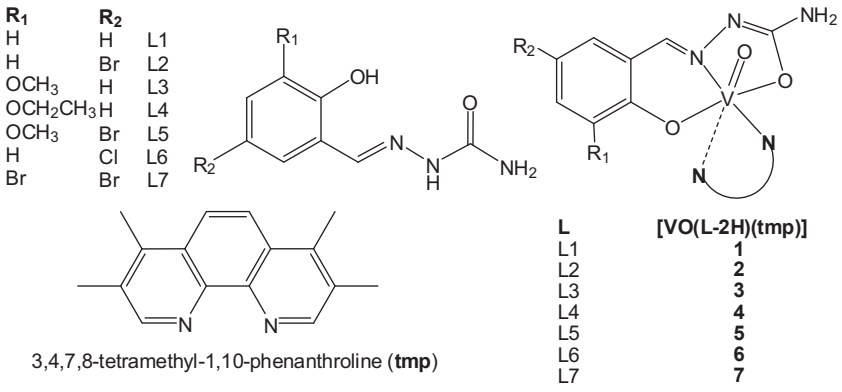

Fig. 1. Salicylaldehyde semicarbazone ligands L1–L7 and new heteroleptic $V^{IV}O$-compounds **1**–**7** including 3,4,7,8 tetramethyl-1,10-phenanthroline (tmp) as co-ligand.

semicarbazone (L6) or 3,5-dibromosalicylaldehyde semicarbazone (L7) and tmp = 3,4,7,8-tetramethyl-1,10-phenanthroline, were synthesized using the following general procedure: 0.375 mmol of L (67 mg L1, 97 mg L2, 78 mg L3, 84 mg L4 or 108 mg L5, 80 mg L6, 127 mg L7) and 0.375 mmol (89 mg) of tmp were suspended in 20 mL of absolute ethanol previously purged with nitrogen for 10 min. [$V^{IV}O(acac)_2$] (0.375 mmol, 100 mg) was dissolved in 5 mL of absolute ethanol, previously purged with nitrogen, and was added to the previous mixture. This was then heated and refluxed under nitrogen for 24 h. The brown-orange solid formed was filtered off from the hot mixture, and washed three times with 2 mL portions of EtOH:Et_2O (1:1).

2.2.1. [$V^{IV}O$(L1-2H)(tmp)]·H_2O, ***1***

Yield: 125 mg, 67%. Anal. calc. for $C_{24}H_{25}N_5O_4V$: C, 57.8; H, 5.1; N, 14.0. Found: C, 57.6; H, 5.1; N, 14.0. ESI-MS (electrospray ionization mass spectra) (MeOH) *m/z* [found (calcd)]: 237.1 (237.14) (25%) $[tmp + H]^+$, 259.1 (259.12) (100%) $[tmp + Na]^+$, 481.3 (481.12) (40%) $[M + H]^+$. Λ_M(DMSO): 4.0 μS/cm^2.

2.2.2. [$V^{IV}O$(L2-2H)(tmp)]·H_2O, ***2***

Yield: 137 mg, 63%. Anal. calc. for $C_{24}H_{24}BrN_5O_4V$: C, 49.9; H, 4.2; N, 12.1. Found: C, 50.1; H, 4.5; N, 11.9. ESI-MS (MeOH) *m/z* [found (calcd)]: 237.1 (237.14) (100%) $[tmp + H]^+$, 259.1 (259.12) (90%) $[tmp + Na]^+$ and 559.1 (559.03) (85%), 560.1 (20%), 561,1 (90%), 562,1 (20%) (Br isotopic pattern) $[M + H]^+$. Λ_M(DMSO): 3.4 μS/cm^2.

2.2.3. [$V^{IV}O$(L3-2H)(tmp)]·H_2O, ***3***

Yield: 125 mg, 63%. Anal. calc. for $C_{25}H_{27}N_5O_5V$: C, 56.8; H, 5.1; N, 13.2. Found: C, 56.6; H, 5.2; N, 13.2. ESI-MS (MeOH) *m/z* [found (calcd)]: 237.1 (237.14) (80%) $[tmp + H]^+$, 259.1 (259.12) (80%) $[tmp + Na]^+$, 511.3 (511.13) (100%) $[M + H]^+$, 555.2 (555.11) (25%) $[M + 2Na–H]^+$. Λ_M(DMSO): 1.6 μS/cm^2.

2.2.4. [$V^{IV}O$(L4-2H)(tmp)]·1/2 H_2O, ***4***

Yield: 127 mg, 65%. Anal. calc. for $C_{26}H_{25}N_5O_3V·½\ H_2O$: C, 58.5; H, 5.3; N, 13.1. Found: C, 58.7; H, 5.0; N, 13.2. ESI-MS (MeOH) *m/z* [found (calcd)]: 237.1 (237.14) (10%) $[tmp + H]^+$, 259.1 (259.12) (60%) $[tmp + Na]^+$, 525.3 (525.15) (65%) $[M + H]^+$. Λ_M(DMSO): 2.0 μS/cm^2.

2.2.5. [$V^{IV}O$(L5-2H)(tmp)], ***5***

Yield: 167 mg, 76%. Anal. calc. for $C_{25}H_{24}BrN_5O_4V$: C, 50.9; H, 4.1; N, 11.9. Found: C, 50.6; H, 4.4; N, 11.5. ESI-MS (MeOH) *m/z* [found (calcd)]: 237.1 (237.14) (30%) $[tmp + H]^+$, 259.1 (259.12) (30%) $[tmp + Na]^+$, 589.0 (589.05) (100%), 590.1 (30%), 591.0 (100%), 592.0 (30%) (Br isotopic pattern) $[M + H]^+$, 611.0 (611.03) (12%) (also shows isotopic Br pattern) $[M + Na]^+$. Λ_M(DMSO): 3.5 μS/cm^2.

2.2.6. [$V^{IV}O$(L6-2H)(tmp)]·H_2O, ***6***

Yield: 97 mg, 48%. Anal. calc. for $C_{24}H_{24}ClN_5O_4V$: C, 54.1; H, 4.5; N, 13.1. Found: C, 54.3; H, 4.8; N, 13.2. ESI-MS (MeOH) *m/z* [found (calcd)]: 237.1 (237.14) (10%) $[tmp + H]^+$, 259.1 (259.12) (100%) $[tmp + Na]^+$ and 515.1 (515.09) (7%), 516.1 (2%) (Cl isotopic pattern) $[M + H]^+$. Λ_M(DMSO): 2.2 μS/cm^2.

2.2.7. [$V^{IV}O$(L7-2H)(tmp)]·H_2O, ***7***

Yield: 137 mg, 56%. Anal. calc. for $C_{24}H_{23}Br_2N_5O_4V$: C, 43.9; H, 3.5; N, 10.7. Found: C, 44.0; H, 3.9; N, 10.3. ESI-MS (MeOH) *m/z* [found (calcd)]: 237.1 (237.14) (60%) $[tmp + H]^+$, 259.1 (259.12) (80%) $[tmp + Na]^+$, 637.1 (636.95) (40%), 638.1 (10%), 639.0 (80%), 640.0 (20%), 641.0 (42%), 642.0 (10%) (2Br isotopic pattern) $[M + H]^+$. Λ_M(DMSO): 1.7 μS/cm^2.

2.3. Physicochemical characterization

C, H and N analyses were carried out with a Thermo Scientific Flash 2000 elemental analyzer. Conductometric measurements were done at 25 °C in 10^{-3} M DMSO solutions using a Conductivity Meter 4310 Jenway [37]. Measurements were done over time in order to access the stability of the complexes in this medium. A 500-MS Varian Ion Trap Mass Spectrometer was used to measure ESI-MS of methanolic solutions of the complexes in the positive mode (after dissolution of the complexes in a very small amount of DMF, N,N-dimethylformamide). A combination of several scans was made for each sample.

The FTIR absorption spectra (4000–300 cm^{-1}) of the complexes and the free ligands were measured as KBr pellets with a Shimadzu IRPrestige-21 instrument. ^{51}V-NMR spectra of *ca.* 3 mM solutions of the complexes in DMF (p.a. grade) (5% D_2O was added) were recorded on a Bruker Avance III 400 MHz instrument. ^{51}V chemical shifts were referenced relative to neat $VOCl_3$ as external standard. EPR spectra were recorded at 77 K with a Bruker ESP 300E X-band spectrometer coupled to a Bruker ER041 X-band frequency meter (9.45 GHz). The complexes were dissolved at room temperature in DMF p.a. grade, previously degassed by passing N_2 for 10 min, to obtain ca. 3 mM solutions. Complexes with non-halogenated semicarbazone ligands showed low solubility and the obtained suspensions were separated by decantation and ~300 μL samples were taken from the clear solutions and immediately frozen in liquid nitrogen for measurement of their EPR spectra. The solutions were allowed to stand under air at room temperature for 24 h after which ^{51}V NMR spectra were measured (5% D_2O was added). For complex **2** several ~300 μL samples were periodically also collected (and frozen in liquid nitrogen) for EPR analysis within 24 h of standing always in contact with air at room temperature. The spin Hamiltonian parameters were obtained by simulation of the spectra with a program developed by Rockenbauer and Korecz [38].

2.4. Biological studies

2.4.1. Anti-T. cruzi activity

T. cruzi epimastigotes (Tulahuen 2 strain) were grown at 28 °C in an axenic medium (BHI-Tryptose) supplemented with 5% fetal bovine serum (FBS) as previously described [39,40]. Cells from a 10-day-old culture (stationary phase) were inoculated into 50 mL of fresh culture milieu to give an initial concentration of 10^6 cells/mL. Cell growth was followed every day by measuring the absorbance of the culture at 600 nm. Before inoculation, the medium was supplemented with the indicated amount of the studied complexes from a freshly prepared stock solution in DMSO. The activity of the co-ligand tmp was also determined. Nifurtimox (Nfx) was used as the reference trypanosomicidal drug. The final concentration of DMSO in the culture medium never exceeded 0.4%, and the control was run in the presence of 0.4% DMSO and in the absence of the studied compounds. No effect on epimastigote growth was observed due to the presence of up to 1% DMSO in the culture milieu.

The percentage of inhibition (PGI) was calculated as follows: PGI (%) = {1 − [(Ap − A0p) / (Ac − A0c)]} × 100, where Ap = $A_{600\ nm}$ of the culture containing the studied compound at day 5; A0p = $A_{600\ nm}$ of the culture containing the studied compound just after addition of the inocula (day 0); Ac = $A_{600\ nm}$ of the culture in the absence of the studied compound (control) at day 5; A0c = $A_{600\ nm}$ in the absence of the studied compound at day 0. To determine IC_{50} values (50% inhibitory concentrations) parasite growth was followed in the absence (control) and presence of increasing concentrations of the corresponding compound. At day 5, the absorbance of the culture was measured and related to the control. The IC_{50} value was taken as the concentration of compound under study necessary to reduce the absorbance ratio to 50%.

2.4.2. Cytotoxicity on mammalian cells

J-774 murine macrophage-like cells (ATCC, USA) were maintained by passage in Dulbecco's modified Eagle's medium (DMEM) containing 4 mM L-glutamine, and supplemented with 10% heat inactivated fetal calf serum and 1% of antibiotics (10,000 U/mL penicillin and 10,000 μg/mL streptomycin). J-774 cells were seeded (1×10^5 cells/

well) in 96 well microplates with 200 μL of RPMI 1640 medium supplemented with 20% heat-inactivated fetal calf serum. Cells were allowed to attach for 48 h in a humidified 5% CO_2/95% air atmosphere at 37 °C and, then, exposed to the studied complexes (1.0–50.0 μM) for 48 h. The cytotoxicity of co-ligands tmp was also determined. Afterwards, cell viability was assessed by measuring the mitochondrial-dependent reduction of 3-(4,5-dimethylthiazol-2-yl)-2,5-diphenyltetrazolium bromide (MTT) (Sigma) to formazan. For that purpose, MTT was added to cells to a final concentration of 0.4 mg/mL and cells were incubated at 37 °C for 3 h. After removing the milieu, formazan crystals were dissolved in DMSO (180 μL), and the absorbance at 595 nm was read using a microplate spectrophotometer.

Cytotoxicity percentages (% C) were determined as follows: $\%C = [100 - (OD_d - OD_{dm}) / (OD_c - OD_{cm})] \times 100$, where OD_d is the mean of $OD_{595\ nm}$ of wells with macrophages and different concentrations of the compounds; OD_{dm} is the mean of $OD_{595\ nm}$ of wells with different compound concentrations in the milieu; OD_c is the growth control and OD_{cm} is the mean of $OD_{595\ nm}$ of wells with milieu only. Results are expressed as IC_{50} (compound concentration that reduces 50% control absorbance at 595 nm). Every reported IC_{50} is the average of three different experiments. The selectivity indexes, SI, were expressed as the ratio between IC_{50} in macrophages and IC_{50} in *T. cruzi* (Tulahuen 2 strain) [41].

2.5. Lipophilicity studies

Reversed-phase TLC experiments were done on precoated TLC plates SIL RP-18W/UV_{254} and eluted with MeOH:DMF:buffer Tris–HCl 10 mM pH 7.4 (85:5:10, v/v/v). Stock solutions were prepared in pure methanol (Aldrich) prior to use. The plates were developed in a closed chromatographic tank, dried and the spots were located under UV light. The R_f values were averaged from two to three determinations, and converted to R_M via the relationship: $R_M = \log_{10}[(1 / R_f) - 1]$ [42–44].

2.6. DNA interaction assessed by computational modeling

The ability to interact with a 20-mer B-DNA duplex of the new seven [VO(L-2H)(tmp)] complexes (**1**–**7** in Fig. 2) and the heads of the other five NN series [VO(L1-2H)(NN)] (NN = phen, bipy, aminophen, epoxyphen, and dppz, respectively identified as **8**–**12** in Fig. 2) was explored by computational modeling combining a density functional theory (DFT) structural characterization of the complexes in solution and ligand–DNA docking.

2.6.1. Preparation of the structure of ligands and B-DNA template

Previous to ligand–DNA docking, the structure of the twelve $V^{IV}O$-complexes under study (**1**–**12** in Fig. 2) was fully optimized in aqueous solution, described by a continuum model (IEF-PCM [45] with Bondi atomic radii [46]). Grimme's UB97-D density functional including dispersion [47] was used with the 6–31 + G(d,p) basis set [48] to describe H/C/N/O/Cl/Br atoms and the LANL2DZ pseudopotential and the associated basis set [49,50] were assigned to vanadium. The nature of all species as minima was verified by analytic Hessian calculations at the same level of theory. All these calculations were done using Gaussian09 rev. D.01 software [51].

Following a docking protocol recently proposed and validated [52–54] to identify two of the main DNA binding modes (intercalation and minor groove recognition) without biases with AutoDock [55,56], a canonical B-DNA template containing a preformed intercalation site at the central base steps of the ds(CAGTGCATA**CG**TGGGCTCCA) 20-mer was built. For this purpose, molecular dynamics simulations (MD) in aqueous solution were run with the AMBER 12 suite [57] on the complex established with ellipticine, a well-known DNA intercalator [58] (see further details on the force fields [59–61] and simulation conditions [62–64] applied in the Supporting information, that includes Fig. S1, displaying the structural features of the DNA template). After ellipticine removal, the resulting DNA structure incorporating the intercalation gap at the **CG** central steps of the duplex was used for docking.

2.6.2. Ligand–DNA duplex docking

All docking studies were done using AutoDock 4.2 [55,56]. Gasteiger–Marsili charges were used [65]. Parameters for V^{IV} were included in AutoDock's parameters file (R_{ii} and $_{ii}$ values for V^{IV} ion were based on AutoDock parameters for transition metals [66]). Since the precise location of the ligands in DNA was unknown, a grid map of $60 \times 60 \times 126$ points with a resolution of 0.675 Å was applied to explore the entire macromolecule surface, with the maps initially centered on the whole DNA 20-mer. Each docking experiment consisted of 25 independent runs, with an initial population of 50 individuals and a maximum of 50×10^6 energy evaluations and 27,000 generations (as optimized by Ricci and Netz [53]). For the remaining parameters, AutoDock 4.2 default values were used. Results differing by less than 2.0 Å in root-square-deviation (RMSd) were grouped into the same cluster. Theoretical dissociation constants (K_d) were calculated from the free energy of binding (ΔG_{bind}) according to the following equation $K_d = \exp(\Delta G_{bind} / RT)$ with T = 298 K. As Huey et al. [56] clearly stated AutoDock 4.2 employs an empirical free energy force field specially designed to estimate ligand–macromolecule binding constants K_b (the inverse of K_d) by capturing both enthalpic and entropic contributions to the formation of the complex in a limited number of terms enabling the calculation of ΔG_{bind}.

3. Results and discussion

Seven new $V^{IV}O$-complexes of the tridentate salicylaldehyde semicarbazone derivatives L1–L7 and tmp as bidentate co-ligand (Fig. 1) were synthesized with reasonable yields. The new compounds were characterized in the solid state and in solution using different techniques. Analytical, TGA, conductimetric, and ESI-MS, FTIR and EPR spectroscopic results are in agreement with the proposed formulation: $[V^{IV}O(L\text{-}2H)(tmp)]\cdot xH_2O$. Their molecular formulae are also depicted in Fig. 1. The compounds are non-conducting in DMSO. ESI-MS experiments confirmed their molecular formulation, as the $M + H^+$ peak was present in the spectra of all compounds. The peaks assigned to the tmp ligand (tmp + H^+ at 237.1) and its sodium adduct (tmp + Na^+ at 259.1) were also present in all spectra. The isotopic patterns due to the presence of one or two Br atoms in complexes **2**, **5** and **7** were identified in the peaks assigned to the metal complexes. The 3:1 isotopic pattern due to the chlorine atom in complex **6** was also observed in the $[M + H]^+$ peak.

3.1. Characterization of the complexes in the solid state

3.1.1. IR spectroscopic studies

Tentative assignments of the main IR bands were made based on our previous reports on vibrational behavior of metal complexes of salicylaldehyde semicarbazone derivatives [26,28,29,31–36,67–69]. Some selected IR bands and their assignment are presented in Table 1. The absence of the ν(C═O) bands, present in the ligands spectra at around 1672–1698 cm^{-1}, indicates the enolization of the amide functionality upon coordination to vanadium. Instead, strong bands at *ca.* 1600–1620 cm^{-1} are observed, which are characteristic of the coordination of the ligand enolate forms [68].

The shift of ν(C═O) and ν(C═N) bands and the absence of the sharp weak phenolic ν(OH) (in the 3430–3500 cm^{-1} region) and of the ν(NH) (in the 3150–3190 cm^{-1} region) bands are in agreement with tridentate coordination of the semicarbazone ligand through the carbonylic oxygen ($O_{C=O}$), the deprotonated azomethyne nitrogen ($N_{azomethyne}$) and the deprotonated phenolic oxygen ($O_{phenolate}$). In addition, the complexes show a characteristic strong peak at around 960 cm^{-1} assigned to ν(V═O). All the spectral modifications observed

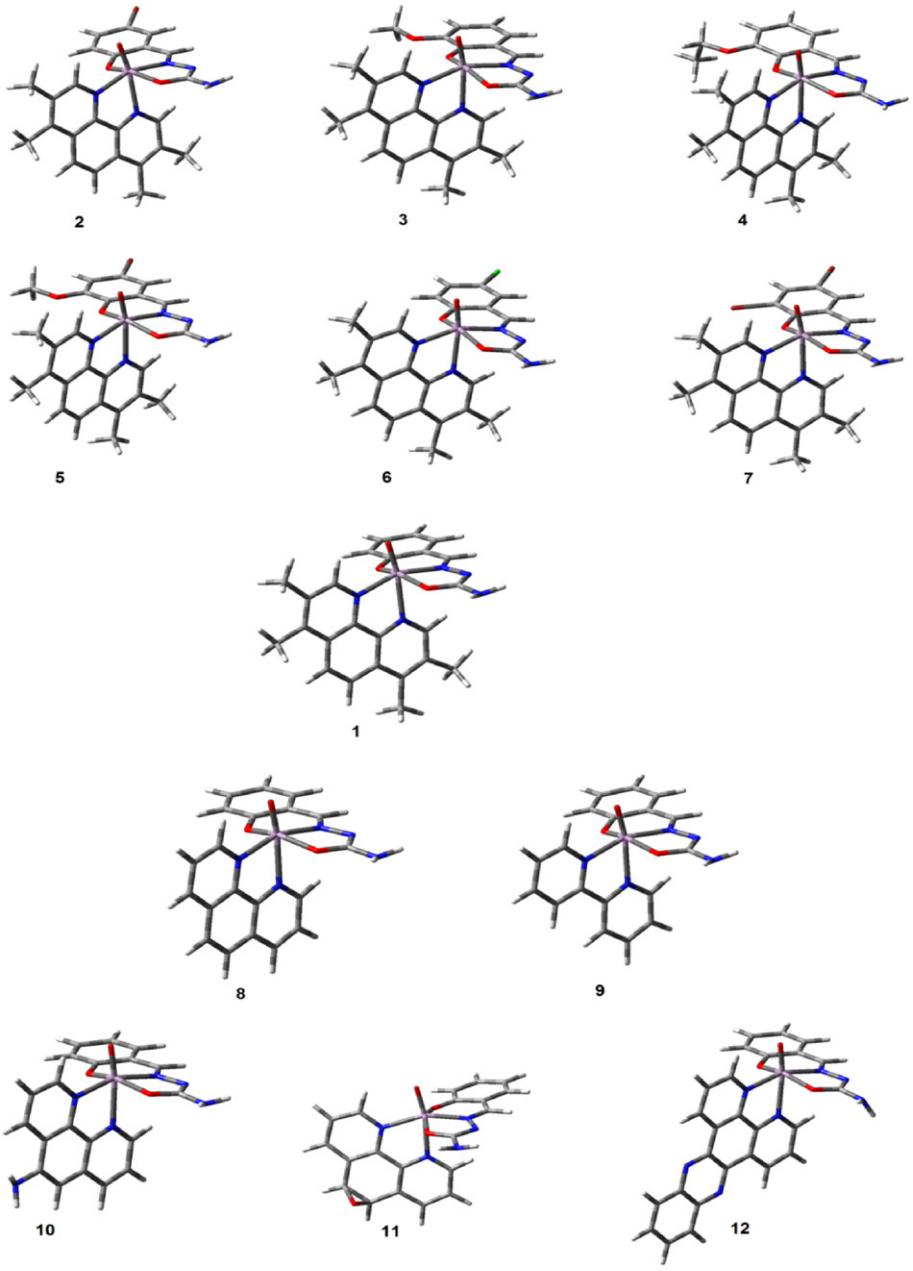

Fig. 2. PCM–DFT structures of the oxidovanadium(IV) complexes modeled in aqueous solution: [VO(L1-2H)(tmp)], **1**, [VO(L2-2H)(tmp)], **2**, [VO(L3-2H)(tmp)], **3**, [VO(L4-2H)(tmp)], **4**, [VO(L5-2H)(tmp)], **5**, [VO(L6-2H)(tmp)], **6**, [VO(L7-2H)(tmp)], **7**, [VO(L1-2H)(phen)], **8**, [VO(L1-2H)(bipy)], **9**, [VO(L1-2H)(aminophen)],**10**, [VO(L1-2H)(epoxyphen)], **11**, and [VO(L1-2H)(dppz)], **12**.

upon complexation agree with those previously reported for other [$V^{IV}O$(L-2H)(NN)] analogous complexes [26,28,31–34].

3.2. Characterization of the complexes in solution

EPR studies were carried out to further characterize the new $V^{IV}O$-complexes. In addition, as the biological activity of the complexes was tested in vitro in aerated diluted solutions and with incubating periods of several days, additional spectroscopic studies were done to understand the stability of the new complexes at room temperature towards hydrolysis and/or oxidation of V^{IV} and to compare it with the equivalent data previously reported for [$V^{IV}O$(L-2H)(NN)] complexes with different NN co-ligands [28,31,32].

Thus, the solutions were prepared and kept at room temperature and samples were periodically collected and frozen in liquid nitrogen. The X-band EPR spectra were measured for DMF solutions at 77 K and are shown in Fig. 3. The EPR spectra are similar for all seven tmp complexes, each depicting a pattern corresponding to the presence of only one species. All spectra were simulated and the determined spin Hamiltonian parameters are included in Table 2.

The g values and hyperfine coupling constants are in agreement with those obtained for related [$V^{IV}O$(L-2H)(NN)] compounds in which NN refers to phen, bipy, dppz, aminophen and epoxyphen: $g_z \sim 1.948 \pm 0.008$ and $A_z \sim 159.8 \pm 0.4 \times 10^{-4}\ cm^{-1}$. These parameters were previously assigned to complexes with binding modes including the semicarbazone as a tridentate ligand bound equatorially by $O_{phenolate}$, $N_{azomethyne}$ and O_{C-O}, and the phenanthroline-type ligands

Table 1
Tentative assignment of selected IR bands of the [$V^{IV}O$(L-2H)(tmp)] complexes **1–7**. Bands for the free semicarbazone ligands L1–L7 are included for comparison. Band positions are given in cm^{-1}.

Compound	ν(VO)	ν(CO)	ν(CN)[a]	ν(OH)	ν(NH)
L1 [22]	–	1695	1593	3493	3155
[$V^{IV}O$(L1-2H)(tmp)], **1**	959	1618	1599	–	–
L2 [22]	–	1698	1596	3470	3170
[$V^{IV}O$(L2-2H)(tmp)], **2**	961	1614	1599	–	–
L3 [22]	–	1676	1586	3466	3160
[$V^{IV}O$(L3-2H)(tmp)], **3**	959	1617	1595	–	–
L4 [22]	–	1667	1593	3433	3160
[$V^{IV}O$(L4-2H)(tmp)], **4**	959	1618	1598	–	–
L5 [22]	–	1672	1572	3477	3191
[$V^{IV}O$(L5-2H)(tmp)], **5**	960	1618	1593	–	–
L6	–	1682	1579	3480	3157
[$V^{IV}O$(L6-2H)(tmp)], **6**	960	1619	1597	–	–
L7	–	1674	1600	3473	3177
[$V^{IV}O$(L7-2H)(tmp)], **7**	961	1611	1593	–	–

Crystallization solvent molecules were not included for simplicity.
[a] The bands assigned to ν(C═N) (azomethine) are associated with the aromatic (C═C) stretching bands [69].

bound as bidentate through the two N donors, in a equatorial–axial mode [26,28,31,32].

In some of the previously reported systems a solvolysis species was often also detected, particularly for the bipy complexes, but in the present cases only one species is clearly identified in the EPR spectra, indicating that besides being resistant to oxidation the solutions of the new tetramethylphenanthroline heteroleptic complexes kept at room temperature are also quite stable towards solvolysis.

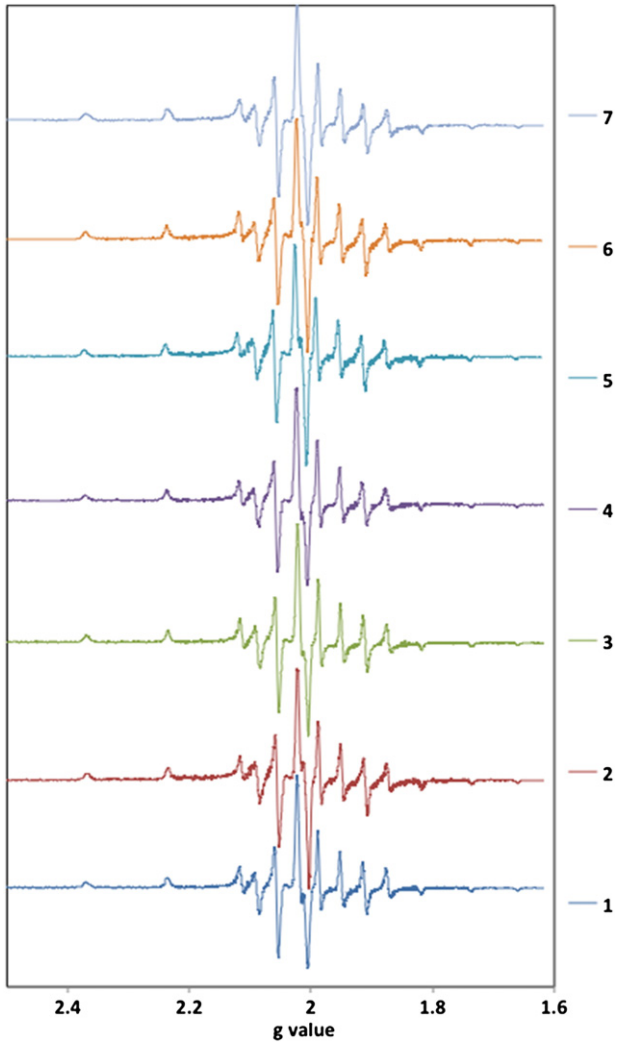

Fig. 3. First derivative of the EPR spectra measured at 77 K for the [VO(L-2H)(tmp)] complexes **1–7** in DMF.

Table 2
Spin Hamiltonian parameters obtained by simulation of the EPR spectra measured at 77 K.

Compound	g_x,g_y	g_z	A_x,$A_y \times 10^4$ cm^{-1}	$A_z \times 10^4$ cm^{-1}
[VO(L1-2H)(tmp)], **1**	1.986	1.953	55.2	159.4
[VO(L2-2H)(tmp)], **2**	1.985	1.952	54.9	159.8
[VO(L3-2H)(tmp)], **3**	1.986	1.954	55.3	159.8
[VO(L4-2H)(tmp)], **4**	1.986	1.954	55.8	159.9
[VO(L5-2H)(tmp)], **5**	1.986	1.952	54.7	159.7
[VO(L6-2H)(tmp)], **6**	1.985	1.952	54.8	159.5
[VO(L7-2H)(tmp)], **7**	1.986	1.953	55.5	160.1

In order to further evaluate the stability towards hydrolysis and/or oxidation of V^{IV}, a solution of complex **2** dissolved in DMF was kept at room temperature over a 24 h period and ~300 μL samples were periodically collected and frozen in liquid nitrogen, and their EPR spectra measured. The obtained spectra are shown in Fig. 4.

As shown in Fig. 4B, there is a slight increase in spectral intensity within the first five hours, that has also been previously observed with this type of complexes due to their slow dissolution. After 24 h the intensity of the spectrum was ca. 85% of the intensity at 5 h, but no new species could be detected by EPR. Overall, it can be concluded that complex **2** shows quite high stability towards hydrolysis and/or oxidation of V^{IV}. This was corroborated by ^{51}V NMR spectroscopy as no peaks due to V^{V}-species were observed after 24 h. Similar behavior can be expected for the other complexes of the series, since 24 h after dissolving the complexes in DMF no color changes were observed and no signals were detected by ^{51}V NMR spectroscopy, indicating that the complexes are stable and do not significantly oxidize within this time frame.

From the solution spectroscopic characterization it can be concluded that the [VO(L-2H)(tmp)] complexes are stable and resistant to solvolysis and oxidation in DMF, similarly to their [VO(L-2H)(aminophen)] and [VO(L-2H)(phen)] analogs [32]. Moreover, they are much more stable than the bipy and epoxyphen complexes, which showed oxidation within hours [28,31,32]. Therefore, upon dissolution in the media, which will be in contact with cells, we anticipate that the complexes will behave similarly.

3.3. Biological results

3.3.1. In vitro anti-T. cruzi activity and unspecific cytotoxicity

The $V^{IV}O$-complexes and the tmp co-ligand were evaluated in vitro for their anti-*T. cruzi* activity against epimastigotes of Tulahuen 2 strain and their selectivity was analyzed using murine macrophages, J-774. Macrophages are among the first cells with which *T. cruzi* has contact in the entry process into a mammalian host. Therefore, they are widely used as mammalian cell models for determining toxicity on mammals and selectivity against parasites [70,71].

The obtained IC_{50} values are included in Table 3. The new salicylaldehyde semicarbazone derivatives L6 and L7 were not active, analogously to previously reported results for L1–L5 ($IC_{50} > 25$ μM) [31].

In molar units all new $V^{IV}O$–vanadium complexes were more active than the reference drug Nifurtimox and four of them more active than tmp. They are among the most active compounds of the whole [$V^{IV}O$(L-2H)(NN)] series. In addition, all showed good selectivity indexes (in the range 10–204), particularly the most active ones. As previously postulated for the other [$V^{IV}O$(L-2H)(NN)] compounds, the complexes of brominated ligands L2, L5 and L7 are the most active and most selective. In addition, the complex of the chlorinated ligand L6 is five times less active than the complex of the brominated analog L2. Four of the complexes are more selective than the free tmp ligand.

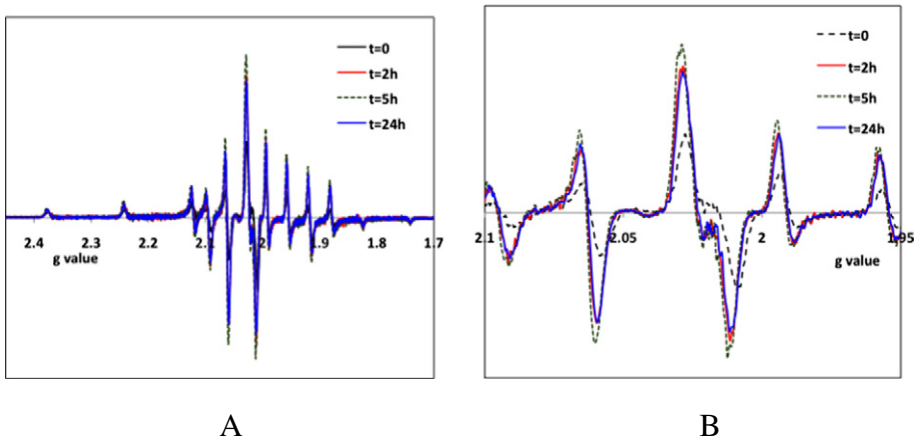

Fig. 4. First derivative of the EPR spectra measured at 77 K for solutions of complex **2** in DMF (3.0 mM). The solution was kept at room temperature in contact with air and samples were periodically collected and frozen at the indicated time periods. A — full field region measured and B — central region of the EPR spectra. The compound is moderately soluble and the intensity of the EPR spectra increased with time up to 5 h. All spectra were measured with the same acquisition parameters: 5 scans, gain = 1.78×10^4, modulation amplitude = 2, time constant and conversion time = 20.48.

Due to their high activity and high selectivity, complexes **2**, **4**, **5** and **7** may be considered new hits for further drug development.

3.4. Lipophilicity studies

Lipophilicity of the new complexes and the free ligands was evaluated using reversed-phase TLC experiments where the stationary phase, precoated TLC-C_{18}, simulates lipids of biological membranes or receptors, and the selected mobile phase resembles the aqueous biological milieu. The composition of the mobile phase, MeOH:DMF:Tris–HCl buffer 10 mM pH 7.4 (85:5:10, v/v/v), is the one previously used to test the other members of the series, thus, allowing comparison of the whole series [31,32]. This methodology is widely accepted by medicinal chemists as an alternative method to evaluate experimental lipophilicity [72]. Table 4 summarizes the R_M values for each tmp compound.

As expected the new complexes are more lipophilic than their phen analogous compounds [31]. In addition, as previously reported for the rest of the series the complexes are more lipophilic than the free tmp and semicarbazone ligands [31,32].

In the QSAR study previously reported for the whole [$V^{IV}O$(L-2H)(NN)] series, [32] we found that the optimal R_M value for maximal anti-*T. cruzi* activity should be close to 1.29. Herein, we confirmed that some of the most active complexes, i.e. **2** and **4**, fit very well this requirement. Other derivatives with values with R_M near this one, i.e. derivative **3** were outliers, probably due to other mechanism(s) of action being determinant to their biological activity.

Table 3
In vitro biological activity on *T. cruzi* (Tulahuen 2 strain) and on macrophages J-774 of the oxidovanadium(IV) complexes, Nifurtimox (Nfx) and the tmp co-ligand. SD values are included.

Compound	IC_{50} (μM) *T. cruzi* (Tulahuen 2)	IC_{50} (μM) J-774 murine macrophages[a]	SI
[$V^{IV}O$(L1-2H)(tmp)], **1**	3.2 ± 0.5	31 ± 3	10
[$V^{IV}O$(L2-2H)(tmp)], **2**	0.27 ± 0.09	25 ± 2	93
[$V^{IV}O$(L3-2H)(tmp)], **3**	3.5 ± 0.9	45 ± 5	13
[$V^{IV}O$(L4-2H)(tmp)], **4**	0.5 ± 0.1	18 ± 1	37
[$V^{IV}O$(L5-2H)(tmp)], **5**	0.25 ± 0.08	51 ± 8	204
[$V^{IV}O$(L6-2H)(tmp)], **6**	1.3 ± 0.3	18 ± 1	12
[$V^{IV}O$(L7-2H)(tmp)], **7**	0.6 ± 0.1	33 ± 3	55
tmp	0.7 ± 0.1	12 ± 1	17
Nfx	7.7 ± 0.3 [32]	316.0 ± 0.5 [41]	41

SI: selectivity index = IC_{50} macrophages (μM)/IC_{50} *T. cruzi*.
[a] Values are the average of three sets of experiments.

3.5. Interaction with DNA as explored by molecular docking

Our strategy of antitrypanosomal vanadium-based drug design has been supported on the development of new heteroleptic vanadium compounds by selection of different NN DNA intercalating co-ligands, aiming DNA as the potential target [26,28,31,32]. Therefore, having now six related [$V^{IV}O$(L-2H)(NN)] series, including six different NN co-ligands and seven salicylaldehyde semicarbazone derivatives (L1–L7), it would be pertinent to compare their DNA interaction ability and to evaluate if the biological activity could be correlated with it, assessing the way this feature is modulated by changes in the nature of both the L-2H and NN co-ligands. For this purpose the interaction mode with DNA for the seven new tmp complexes **1**–**7** as well as for the five previous heads of series (L = L1) identified as species **8**–**12** in Fig. 2, was determined and compared through computational modeling with the corresponding tmp new complex.

3.5.1. Ligand–DNA binding mode and strength

The binding modes resulting from DNA docking are shown in Figs. 5 and 6, superimposed by groups of compounds to facilitate a comparison of the predicted binding modes within the tmp series (compounds **1**–**7**, Fig. 5A) and across the heads of each of the six [$V^{IV}O$(L1-2H)(NN)] series (compounds **1** and **8**–**12**, Figs. 5B and 6). The relative strength of each DNA-interaction across the whole **1**–**12** series, as predicted by AutoDock, is reported in Table 5.

Compounds **9** and **12**, heads of the NN = bipy and dppz series, are taken here as benchmark for assessing the predictive capacity of the docking experiments by comparison to the well-documented behavior of octahedral Ru^{II} species: $[Ru(bipy)_2dppz]^{2+}$ and $[Ru(phen)_2dppz]^{2+}$ are known to strongly interact with DNA by intercalating the dppz moiety between two base pairs [58,73,74] while $[Ru(bipy)_3]^{2+}$ does not

Table 4
R_M values obtained for the $V^{IV}O$-complexes **1**–**7**. The values for the free semicarbazones, tmp and Nfx are included for comparison.

Compound	R_M	Compound	R_M
[$V^{IV}O$(L1-2H)(tmp)], **1**	1.38	L1	−0.75 [31]
[$V^{IV}O$(L2-2H)(tmp)], **2**	1.21	L2	−0.75 [31]
[$V^{IV}O$(L3-2H)(tmp)], **3**	1.19	L3	−0.035 [31]
[$V^{IV}O$(L4-2H)(tmp)], **4**	1.20	L4	−0.66 [31]
[$V^{IV}O$(L5-2H)(tmp)], **5**	1.17	L5	0.12 [31]
[$V^{IV}O$(L6-2H)(tmp)], **6**	1.18	L6	−0.67
[$V^{IV}O$(L7-2H)(tmp)], **7**	0.77	L7	−0.78
tmp	−0.055	Nfx	1.22 [31]

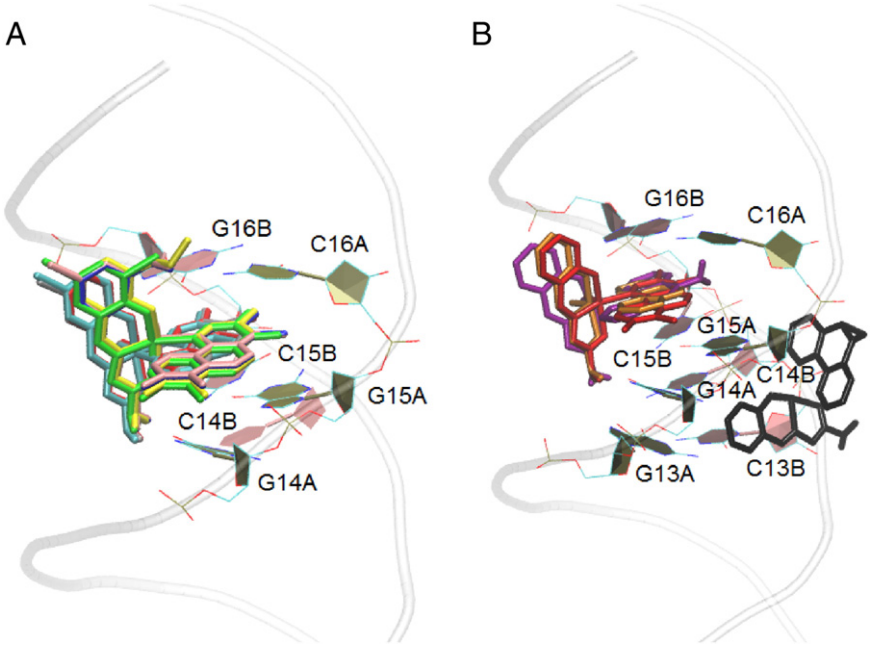

Fig. 5. Predicted DNA-binding mode as compared within and across series. (A) Compounds **1**–**7**. Color code: **1** red, **2** cyan, **3** blue, **4** yellow, **5** pink, **6** gray, **7** green. (B) Compounds **1**, and **8**–**11**. Color code: **1** red, **8** orange, **10** purple, **11** black. DNA strands A/B are evidenced in the nucleobase labels. The binding mode of compounds **9** and **12** is shown in Fig. 6.

intercalate at all, even at micromolar concentrations [58,75], showing that they correctly discriminate between DNA groove binders (**9**, Fig. 6B) and intercalators (**12**, Fig. 6A).

The dppz moiety of **12** appears deeply intercalated in the DNA minor groove between G15A/C16A, slightly angled and protruding from the base-pair stack into the major groove (Fig. 6A), closely resembling the intercalation mode of Λ-$[Ru(phen)_2dppz]^{2+}$ at a GG site [76]. Compound **9** binds into the minor groove near the 5′ end of the DNA 20-mer, rich in G … C steps. In both cases the $-NH_2$ group present in the L1 moiety donates hydrogen-bond to O atoms from G14A (Fig. 6A) or from A4B's phosphate (Fig. 6B). Compounds **1**–**7**, **8**, and **10** all display a wedge-like partial intercalation mode (Fig. 5), approaching DNA from the minor groove as **12**, but with the phen moiety of each NN co-ligand contacting G15B/C16B and the rest of the ring exposed to the solvent (see further details in Fig. S2 in the SI), in accordance with the intercalating mode reported for Λ-$[Ru(phen)_3]^{2+}$ [77]. Finally, bearing epoxyphen as NN co-ligand makes **11** a minor groove binder (Fig. 5B) such as **9**, but placed immediately above the intercalation

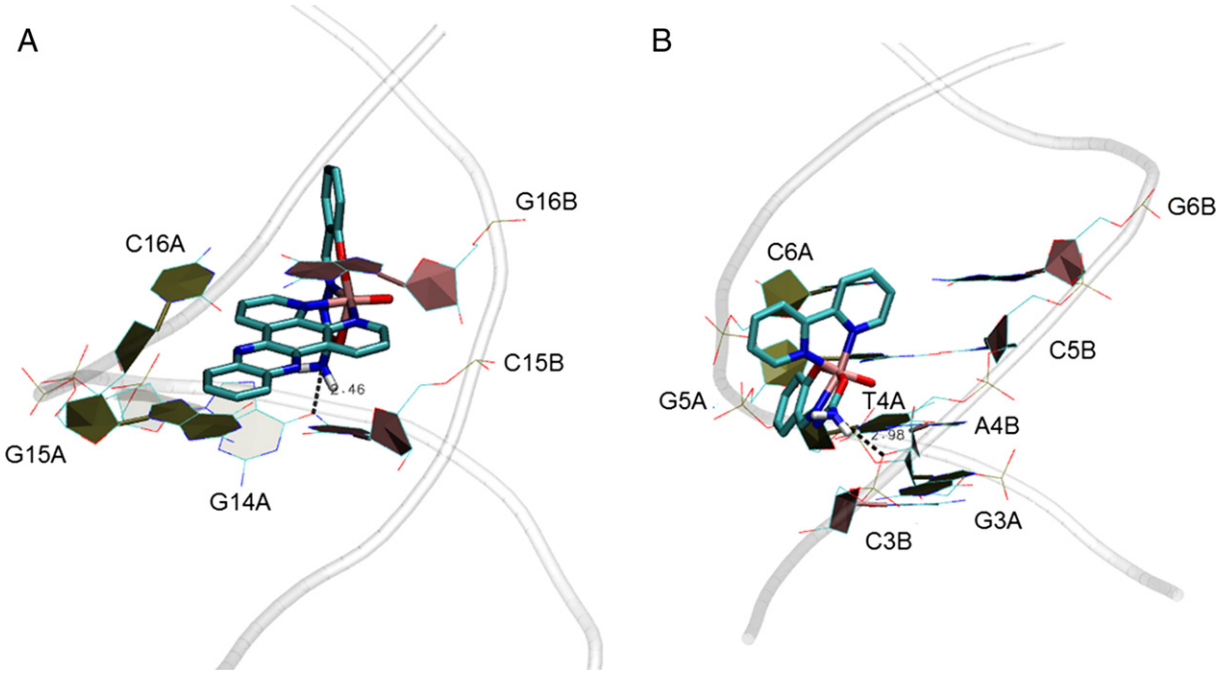

Fig. 6. Predicted DNA-binding mode for [$V^{IV}O$(L1-2H)(dppz)], **12** (A) and [$V^{IV}O$(L1-2H)(bipy)], **9** (B) considered as benchmarks for determining the reliability of the docking model to correctly discriminate between intercalators and groove binders.

Table 5
Trends on the strength of the ligand–DNA interaction for species **1**–**12** in terms of binding free energies (ΔG_{bind}) and dissociation constants (K_d) as predicted by AutoDock 4.2.[a]

Species	ΔG_{bind} (kcal/mol)	K_d (M)
[$V^{IV}O$(L1-2H)(tmp)] **1**	−9.2	1.79×10^{-7}
[$V^{IV}O$(L2-2H)(tmp)] **2**	−9.1	2.19×10^{-7}
[$V^{IV}O$(L3-2H)(tmp)] **3**	−8.3	7.65×10^{-7}
[$V^{IV}O$(L4-2H)(tmp)] **4**	−8.5	5.64×10^{-7}
[$V^{IV}O$(L5-2H)(tmp)] **5**	−8.7	3.89×10^{-7}
[$V^{IV}O$(L6-2H)(tmp)] **6**	−9.3	1.51×10^{-7}
[$V^{IV}O$(L7-2H)(tmp)] **7**	−8.6	5.28×10^{-7}
[$V^{IV}O$(L1-2H)(phen)] **8**	−7.8	1.90×10^{-6}
[$V^{IV}O$(L1-2H)(bipy)] **9**	−7.0	3.97×10^{-5}
[$V^{IV}O$(L1-2H)(aminophen)] **10**	−7.8	1.90×10^{-6}
[$V^{IV}O$(L1-2H)(epoxyphen)] **11**	−6.6	1.44×10^{-5}
[$V^{IV}O$(L1-2H)(dppz)], **12**	−10	4.63×10^{-8}

[a] See Section 2.6.2 for a description and references on the calculation of these magnitudes.

gap, at a G … C rich site almost central in the DNA 20-mer. This shows how phen replacement by epoxyphen impairs the intercalative ability of the co-ligand. All this evidence globally confirms that the nature of the NN co-ligand is the main factor in defining the DNA binding mode of these species.

Regarding the strength of the DNA interactions predicted by molecular docking, it is worth to recall here that whereas AutoDock 4.2 scoring functions are of value to compare relative binding affinities in a series of similar compounds, they have been shown to overemphasize H-bonding (eventually favoring as top scores structures with RMSd > 2 Å from the available crystal structures [52,53]). Thus a quantitative use of the binding affinities in Table 5 as predictors to discriminate between species with dissimilar DNA binding modes is not advised. The top scoring structures reported here are good to qualitatively evaluate unknown binding modes and as a starting point for determination of ΔG_{bind} with more sophisticated modeling methods.

In general terms, minor groove DNA binders **9** and **11** are those with lower affinity (predicted highest K_d values) in agreement with experiments on related Ru^{II} complexes [58]. Among the minor groove intercalators, compound **12** establishes the strongest interaction with DNA through dppz co-ligand, followed by the new seven species corresponding to the tmp series (**1**–**7**). Tetramethyl substitution in phen appears to confer **1**–**7** enhanced affinity towards DNA with respect to **8**. The substitution on the phenol moiety of the semicarbazone ligand along the [$V^{IV}O$(L-2H)(tmp)] series seems to have very low incidence on the DNA affinity when introduced at the R2 position (**1**, **2**, and **6** in Fig. 5A and Table 5), being the effects more appreciable when introduced at R1, resulting in a diminished DNA-affinity (**3**–**5** and **7**, Fig. 5A and Table 5). Contrasting the DNA affinity data in Table 5 with the biological anti-*T. cruzi* activity reported for the tmp series in Table 3 and for the other five NN series in references [31] and [32], no clear correlation is found among both sets, suggesting that although most of the species under study display good DNA intercalating capacity (improved at the seven new compounds) DNA noncovalent interaction would not explain the observed profiles of biological activity for these species. Further research focusing on the identification of the key features of the mechanism of action underlying the high activity and selectivity of the new hits for drug development reported here is needed and has been undertaken by us conducting a more complete computational screening of the properties of the six [$V^{IV}O$(L-2H)(tmp)], which is currently under progress.

4. Conclusions

The previous series of heteroleptic $V^{IV}O$-complexes, [$V^{IV}O$(L-2H)(NN)], including tridentate salicylaldehyde semicarbazone derivatives as ligands (L = L1–L5) and different polypyridyl co-ligands NN, was expanded. A new series of [$V^{IV}O$(L-2H)(tmp)], where tmp = 3,4,7,8-tetramethyl-1,10-phenanthroline and L = L1–L5 or the new halogenated derivatives 5-chlorosalicylaldehyde semicarbazone (L6) or 3,5-dibromosalicylaldehyde semicarbazone (L7), was synthesized and characterized in the solid state and in solution by a combination of techniques. As in the previous series, the V^{IV}-center is in octahedral environment with the tmp ligand coordinated in an equatorial–axial mode and the tridentate semicarbazone ligand occupying the remaining equatorial positions.

The new complexes showed IC_{50} values in the low micromolar or submicromolar range against *T. cruzi* epimastigotes. They were more toxic to the parasite than most of the previously reported analogs and the anti-trypanosomal drug Nifurtimox. Additionally, the new series of compounds displayed good to high selectivities towards the parasite. The complexes of the brominated ligands L2, L5 and L7 showed the lowest IC_{50} values and the highest selectivity indexes.

A deeper insight into the mechanism of DNA interaction of the complexes was gained from molecular docking, suggesting that although the new species are good intercalators, DNA would not be the sole molecular target explaining the observed high activity and selectivity. Further research is currently ongoing to gain more insight on the possible mechanism of action.

The lipophilicity seems to play a relevant role in the bioactivity of the new compounds in agreement with the QSAR study, previously described by us, that involved 25 structurally related [$V^{IV}O$(L-2H)(NN)] complexes with five different NN-ligands.

Acknowledgments

G.S., J.B. and S.R. wish to thank Programa de Apoyo a la Investigación Estudiantil, ID 187, 2013 (CSIC, Uruguay). E.B. and J.V. wish to thank ANII (Uruguay) for their scholarships. J.C.P. and I.C. would like to thank the Fundação para a Ciência e Tecnologia (UID/QUI/00100/2013) for funding (program Investigador FCT, IF/00841/2012), the Portuguese NMR Network (IST-UTL Center), RECI/QEQ-QIN/0189/2012 and PEst-OE/QUI/UI0100/2013.

Appendix A. Supplementary data

Supplementary data to this article can be found online at http://dx.doi.org/10.1016/j.jinorgbio.2015.03.002.

References

[1] A.J. Romanha, S. Lisboa de Castro, M. de Nazaré Correia Soeiro, J. Lannes-Vieira, I. Ribeiro, A. Talvani, B. Bourdin, B. Blum, B. Olivieri, C. Zani, C. Spadafora, E. Chiari, E. Chatelain, G. Chaves, J.E. Calzada, J.M. Bustamante, L. Freitas-Junior, L. Romero, M.T. Bahia, M. Lotrowska, M. Soares, S. Gumes Andrade, T. Armstrong, W. Degrave, Z. de Araújo Andrade, Mem. Inst. Oswaldo Cruz 105 (2010) 233–238.
[2] J.D. Maya, B.K. Cassels, P. Iturriaga-Vásquez, J. Ferreira, M. Faúndez, N. Galanti, A. Ferreira, A. Morello, Comp. Biochem. Physiol. A 146 (2007) 601–620.
[3] I. Ribeiro, A.M. Sevcsik, F. Alves, G. Diap, R. Don, M.O. Harhay, S. Chang, B. Pecoul, PLoS Negl. Trop. Dis. 3 (2009) e484, http://dx.doi.org/10.1371/journal.pntd.0000484.
[4] A. Rassi Jr., A. Rassi, J.A. Marin-Neto, Lancet 375 (2010) 1388–1402.
[5] C.M. Beaumier, P.M. Gillespie, P.J. Hotez, M.E. Bottazzi, Transl. Res. 162 (2013) 144–155.
[6] R.A. Sánchez-Delgado, A. Anzellotti, L. Suárez, in: H. Sigel, A. Sigel (Eds.), Metal ions in biological systems, 41: Metal Ions and Their Complexes in MedicationMarcel Dekker, New York, 2004, pp. 379–419.
[7] S.P. Fricker, R.M. Mosi, B.R. Cameron, I. Baird, Y. Zhu, V. Anastassov, J. Cox, P.S. Doyle, E. Hansell, G. Lau, J. Langille, M. Olsen, L. Qin, R. Skerlj, R.S.Y. Wong, Z. Santucci, J.H. McKerrow, J. Inorg. Biochem. 102 (2008) 1839–1845.
[8] D. Gambino, L. Otero, Inorg. Chim. Acta 393 (2012) 103–114.
[9] M. Navarro, G. Gabbiani, L. Messori, D. Gambino, Drug Discov. Today 15 (2010) 1070–1077.
[10] C. Biot, W. Castro, C. Botté, M. Navarro, Dalton Trans. 41 (2012) 6335–6349.
[11] J. Costa Pessoa, S. Etcheverry, D. Gambino, Coord. Chem. Rev. (2014) http://dx.doi.org/10.1016/j.ccr.2014.12.002.
[12] D. Rehder, Dalton Trans. 42 (2013) 11749.
[13] D. Rehder, Biological activities of V and Cr, in: Jan Reedijk, Kenneth Poeppelmeier (Eds.),Comprehensive Inorganic Chemistry II, Vol. 3, Elsevier, Oxford, 2013, pp. 819–834.
[14] J. Costa Pessoa, I. Tomaz, Curr. Med. Chem. 17 (2010) 3701.

[15] G.R. Willsky, L.H. Chi, M. Godzala, P.J. Kostyniak, J.J. Smee, A.M. Trujillo, J.A. Alfano, W.J. Ding, Z.H. Hu, D.C. Crans, Coord. Chem. Rev. 255 (2011) 2258.
[16] D. Rehder, Future Med. Chem. 4 (2012) 1823.
[17] D. Rehder, in: A. Sigel, et al., (Eds.), Interrelations between essential metal ions and human diseases, Metal Ions in Life Sciences, 13, © Springer Science + Business Media, Dordrecht, 2014http://dx.doi.org/10.1007/978-94-007-7500-8_5.
[18] D. Gambino, Coord. Chem. Rev. 255 (2011) 2193.
[19] K. Kinnamon, E.A. Steck, E.S. Rane, Antimicrob. Agents Chemother. 15 (1979) 157.
[20] Y. Dong, R.K. Narla, E. Sudbeck, F.M. Uckun, J. Inorg. Biochem. 78 (2000) 321.
[21] J. Lu, H. Guo, X. Zeng, Y. Zhang, P. Zhao, J. Jiang, L. Zang, J. Inorg. Biochem. 112 (2012) 39–48.
[22] P.B. Sreeja, M.R. Prathapachandra Kurup, Spectrochim. Acta A 61 (2005) 331–336.
[23] P.K. Sasmal, Ashis K. Patra, M. Nethaji, A.R. Chakravarty, Inorg. Chem. 46 (2007) 11112–11121.
[24] P. Prasad, P.K. Sasmal, I. Khan, P. Kondaiah, A.R. Chakravarty, Inorg. Chim. Acta 372 (2011) 79–87.
[25] I.E. León, N. Butenko, A.L. Di Virgilio, C.I. Muglia, E.J. Baran, I. Cavaco, S.B. Etcheverry, J. Inorg. Biochem. 134 (2014) 106–117.
[26] J. Benítez, L. Guggeri, I. Tomaz, J. Costa Pessoa, V. Moreno, J. Lorenzo, F.X. Avilés, B. Garat, D. Gambino, J. Inorg. Biochem. 103 (2009) 1386–1394.
[27] J. Benítez, L. Guggeri, I. Tomaz, G. Arrambide, M. Navarro, J. Costa Pessoa, B. Garat, D. Gambino, J. Inorg. Biochem. 103 (2009) 609–616.
[28] J. Benítez, L. Becco, I. Correia, S. Milena Leal, H. Guiset, J. Costa Pessoa, J. Lorenzo, S. Tanco, P. Escobar, V. Moreno, B. Garat, D. Gambino, J. Inorg. Biochem. 105 (2011) 303–311.
[29] J. Benítez, I. Correia, L. Becco, M. Fernández, B. Garat, H. Gallardo, G. Conte, M.L. Kuznetsov, A. Neves, V. Moreno, J. Costa Pessoa, D. Gambino, Z. Anorg. Allg. Chem. 639 (2013) 1417–1425.
[30] J. Benítez, A. Cavalcanti de Queiroz, I. Correia, M. Amaral Alves, M.S. Alexandre-Moreira, E.J. Barreiro, L. Moreira Lima, J. Varela, M. González, H. Cerecetto, V. Moreno, J. Costa Pessoa, D. Gambino, Eur. J. Med. Chem. 62 (2013) 20–27.
[31] M. Fernández, L. Becco, I. Correia, J. Benítez, O.E. Piro, G.A. Echeverria, A. Medeiros, M. Comini, M.L. Lavaggi, M. González, H. Cerecetto, V. Moreno, J. Costa Pessoa, B. Garat, D. Gambino, J. Inorg. Biochem. 127 (2013) 150–160.
[32] M. Fernández, J. Varela, I. Correia, E. Birriel, J. Castiglioni, V. Moreno, J. Costa Pessoa, H. Cerecetto, M. González, D. Gambino, Dalton Trans. 42 (2013) 11900–11911.
[33] P. Noblía, E.J. Baran, L. Otero, P. Draper, H. Cerecetto, M. González, O.E. Piro, E.E. Castellano, T. Inohara, Y. Adachi, H. Sakurai, D. Gambino, Eur. J. Inorg. Chem. 322–328 (2004).
[34] P. Noblía, M. Vieites, P. Parajón-Costa, E.J. Baran, H. Cerecetto, P. Draper, M. González, O.E. Piro, E.E. Castellano, A. Azqueta, A. López, A. Monge-Vega, D. Gambino, J. Inorg. Biochem. 99 (2005) 443–451.
[35] J. Rivadeneira, D. Barrio, G. Arrambide, D. Gambino, L. Bruzzone, S. Etcheverry, J. Inorg. Biochem. 103 (2009) 633–642.
[36] D. Gambino, M. Fernández, D. Santos, G.A. Etcheverría, O.E. Piro, F.R. Pavan, C.Q.F. Leite, I. Tomaz, F. Marques, Polyhedron 30 (2011) 1360–1366.
[37] W.J. Geary, Coord. Chem. Rev. 7 (1971) 81–91.
[38] A. Rockenbauer, L. Korecz, Appl. Magn. Reson. 10 (1996) 29–43.
[39] J. Varela, M.L. Lavaggi, M. Cabrera, A. Rodríguez, P. Miño, X. Chiriboga, H. Cerecetto, M. González, Nat. Prod. Commun. 7 (2012) 1139–1142.
[40] P. Hernández, P. Hernández, R. Rojas, R.H. Gilman, M. Sauvain, L.M. Lima, E.J. Barreiro, M. González, H. Cerecetto, Eur. J. Med. Chem. (2012) 64–74.
[41] A. Gerpe, G. Álvarez, D. Benitez, L. Boiani, M. Quiroga, P. Hernández, M. Sortino, S. Zacchino, M. González, H. Cerecetto, Bioorg. Med. Chem. 17 (2009) 7500–7509.
[42] C. Hansch, A. Leo, The hydrophobic parameter: measurement and calculation; in exploring QSAR. Fundamentals and Applications in Chemistry and Biology, American Chemical Society Ed., Washington, 1995, pp. 97–124.
[43] H. Cerecetto, R. Di Maio, M. González, M. Risso, P. Saenz, G. Seoane, A. Denicola, G. Peluffo, C. Quijano, C. Olea-Azar, J. Med. Chem. 42 (1999) 1941–1950.
[44] C. Urquiola, M. Vieites, G. Aguirre, A. Marín, B. Solano, G. Arrambide, P. Noblía, M.L. Lavaggi, M.H. Torre, M. González, A. Monge, D. Gambino, H. Cerecetto, Bioorg. Med. Chem. 14 (2006) 5503–5509.
[45] E. Cancès, B. Mennucci, J. Tomasi, J. Chem. Phys. 107 (1997) 3032–3041.
[46] A. Bondi, J. Phys. Chem. 68 (1964) 441–451.
[47] S. Grimme, J. Comput. Chem. 27 (2006) 1787–1799.
[48] R. Ditchfield, W.J. Hehre, J.A. Pople, J. Chem. Phys. 54 (1971) 724–728.
[49] P.J. Hay, W.R. Wadt, J. Chem. Phys. 82 (1985) 270–283.
[50] P.J. Hay, W.R. Wadt, J. Chem. Phys. 82 (1985) 299–310.
[51] M.J. Frisch, G.W. Trucks, H.B. Schlegel, et al., Gaussian 09, Revision D.01, Gaussian Inc., Wallingford CT, 2009.
[52] Y. Gilad, H. Senderowitz, J. Chem. Inf. Model. 54 (2014) 96–107.
[53] C.G. Ricci, P.A. Netz, J. Chem. Inf. Model. 49 (2009) 1925–1935.
[54] P.A. Holt, J.B. Chaires, J.O. Trent, J. Chem. Inf. Model. 48 (2008) 1602–1615.
[55] G.M. Morris, R. Huey, W. Lindstrom, M.F. Sanner, R.K. Belew, D.S. Goodsell, A.J. Olson, J. Comput. Chem. 30 (2009) 2785–2791.
[56] R. Huey, G.M. Morris, A.J. Olson, D.S. Goodsell, J. Comput. Chem. 28 (2007) 1145–1152.
[57] D.A. Case, T.A. Darden, T.E. Cheatham III, C.L. Simmerling, J. Wang, R.E. Duke, R. Luo, R.C. Walker, W. Zhang, K.M. Merz, P.A. Kollman, et al., AMBER 12, University of California, San Francisco, 2012.
[58] A. Mihailovic, I. Vladescu, M. McCauley, Langmuir 22 (2006) 4699–4709.
[59] A. Pérez, I. Marchán, D. Svozil, J. Sponer, T.E. Cheatham III, C.A. Laughton, M. Orozco, Biophys. J. 92 (2007) 3817–3829.
[60] J. Wang, R.M. Wolf, J.W. Caldwell, P.A. Kollman, D.A. Case, J. Comput. Chem. 25 (2004) 1157–1174.
[61] C.M. Breneman, K.B. Wiberg, J. Comput. Chem. 11 (1990) 361–373.
[62] U. Essmann, L. Perera, M.L. Berkowitz, T. Darden, H. Lee, L.G. Pedersen, J. Chem. Phys. 103 (1995) 8577–8593.
[63] H.J.C. Berendsen, J.P.M. Postma, W.F. van Gunsteren, A. DiNola, J.R. Haak, J. Chem. Phys. 81 (1984) 3584–3690.
[64] J.P. Ryckaert, G. Ciccotti, H.J.C. Berendsen, J. Comput. Phys. 23 (1977) 327–341.
[65] J. Gasteiger, M. Marsili, Tetrahedron 36 (1980) 3219–3228.
[66] Autodock Forum, ADL: Parameters for docking with metal ions in receptor, http://autodock.1369657.n2.nabble.com/ADL-Parameters-for-docking-with-metal-ions-in-receptor-td2505649.html (Accessed May 2014).
[67] I. Machado, S. Fernández, L. Becco, B. Garat, J.S. Gancheff, A. Rey, D. Gambino, J. Coord. Chem. 67 (2014) 1835–1850.
[68] S. Nica, M. Rudolph, H. Gorls, W. Plass, Inorg. Chim. Acta 360 (2007) 1743–1752.
[69] J. Costa Pessoa, M.J. Calhorda, I. Cavaco, I. Correia, M.T. Duarte, V. Felix, R.T. Henriques, M.F.M. Piedade, I. Tomaz, J. Chem. Soc. Dalton Trans. (2002) 4407–4415.
[70] D. Benitez, M. Cabrera, P. Hernández, L. Boiani, M.L. Lavaggi, R. Di Maio, G. Yaluff, E. Serna, S. Torres, M.E. Ferreira, N. Vera de Bilbao, E. Torres, S. Pérez-Silanes, B. Solano, E. Moreno, I. Aldana, A. López de Ceráin, H. Cerecetto, M. González, A. Monge, J. Med. Chem. 54 (2011) 3624–3636.
[71] M. Cabrera, M.L. Lavaggi, P. Hernández, A. Merlino, A. Gerpe, W. Porcal, M. Boiani, A. Ferreira, A. Monge, A.L. de Cerain, M. González, H. Cerecetto, Toxicol. Lett. 190 (2009) 140–149.
[72] C. Giaginis, A. Tsantili-Kakoulidou, Alternative measures of lipophilicity: from octanol–water partitioning to IAM retention, J. Pharm. Sci. 97 (2008) 2984–3004.
[73] C.M. Dupureur, J.K. Barton, Inorg. Chem. 36 (1997) 33–43.
[74] I. Haq, P. Lincoln, D. Suh, B. Nordén, B. Chowdhry, J.B. Chaires, J. Am. Chem. Soc. 117 (1995) 4788–4796.
[75] A.M. Pyle, J.P. Rehmann, R. Meshoyrer, C.V. Kumar, N.J. Turro, J.K. Barton, J. Am. Chem. Soc. 111 (1989) 3051–3058.
[76] H. Niyazi, J.P. Hall, K. O'Sullivan, G. Winter, T. Sorensen, J.M. Kelly, C.J. Cardin, Nat. Chem. 4 (2012) 621–628.
[77] A. Reymer, B. Nordén, Chem. Commun. 48 (2012) 4941–4943.